MIT
International Center for
Air Transportation

FLIGHT TEST RESULTS OF A SUBSCALE SUPER-STOL AIRCRAFT

Christopher B. Courtin, R. John Hansman, Mark Drela

This report presents research published under the same title at the 2020 American Institute of Aeronautics and Astronautics (AIAA) Scitech forum. Citations should be made to the original work

Report No. ICAT-2020-01
January 2020

MIT International Center for Air Transportation (ICAT)
Department of Aeronautics & Astronautics
Massachusetts Institute of Technology
Cambridge, MA 02139 USA

Flight Test Results of a Subscale Super-STOL Aircraft

Christopher Courtin*, John Hansman†, Mark Drela‡
Massachusetts Institute of Technology, Cambridge, 02139, USA

This paper presents the results from initial flight tests of a 30% scale demonstrator of a blown-wing SuperSTOL concept aircraft, intended for operation from extremely short runways of 100 ft or less. The subscale demonstrator is aimed at investigating the maximum achievable in-flight lift coefficients with the blown wing, as well as the control and handling qualities with a mostly conventional aircraft configuration with unblown control surfaces. With a relatively modest amount of blowing power - a static thrust/weight of 0.45 - the flight tests show that the blown wing SuperSTOL concept can generate high lift coefficients greater than 10 in flight. It was observed that reducing the size of the propeller enabled larger C_L values to be achieved. In high-C_L flight the roll control authority of conventional ailerons was found to be marginal, partly due to the low fight dynamic pressure and partly due to the local stall over the unblown part of the aileron. In the configuration tested most of the elevator deflection was consumed to obtain pitch trim at low speed. A finite rotation rate to takeoff attitude was found to significantly contribute to the ground roll distance.

I. Nomenclature

c	airfoil chord
c_ℓ	2D airfoil lift coefficient
C_L	3D lift coefficient
C_X	3D net streamwise force coeff. ($= C_D - C_T$)
Δc_J	2D jet momentum-excess coefficient
ΔC_J	3D jet momentum-excess coefficient
E	total aircraft energy
h	flight altitude
h_d	2D propulsor disk height
S	reference area
V	flight speed
V_J	propeller jet speed
W	overall weight
α	angle of attack
γ	flight path angle
ρ	air density
Ω	propeller rotation rate

II. Introduction

Recent work [1] [2] has proposed the use of super-short takeoff and landing (SSTOL) aircraft for urban passenger transport missions. The SSTOL concept is a fixed wing vehicle which has infrastructure requirements that are competitive with vertical takeoff and landing (VTOL) aircraft. Compared to the VTOL vehicles being widely proposed, SSTOL may offer advantages in terms of both certification and performance.

Certification challenges for most distributed electric propulsion VTOL aircraft may arise from the fact that the propulsion system in hover provides both lift and attitude control. This coupling increases the criticality of power system failures, as well as requiring a fly-by-wire control system. This requires increased redundancy and complexity, adding cost and weight to the aircraft and time to the certification process [3]. A fixed-wing SSTOL aircraft, with an unpowered stall speed of less than 61 kts, would be comparable to existing single-engine aircraft in a common mode power system failure scenario, providing an established certification pathway. Additionally, due to the lower required thrust-to-weight ratio and improved cruise L/D of SSTOL aircraft, there are likely performance benefits in terms of range, cruise speed, and/or passengers capability for a given vehicle weight. If takeoff and landing distances can be made comparable to the size of a vertiport, there may be substantial benefit to using SSTOL aircraft for many of the proposed urban air mobility missions.

Distributed electric propulsion technology enables extreme short field performance because it is an efficient and mechanically simple means of having externally blown flaps along most of the wing span. The blowing jet is created by electric motors arranged along and under the leading edge of the wing; this jet enhances the lift of the wing through

*Graduate Student, Department of Aeronautics and Astronautics, AIAA Member
†T. Wilson Professor, Department of Aeronautics and Astronautics, AIAA Fellow.
‡Terry J. Kohler Professor, Department of Aeronautics and Astronautics, AIAA Fellow.

interaction with the trailing edge flaps. Wind tunnel test of a wing section based on this concept have demonstrated two-dimensional wing section $c_\ell \simeq 9$ at reasonable blowing power levels [4].

Using relatively simple 3D corrections to the wind tunnel data, it is estimated that takeoff and landing ground rolls of less than 100 ft. can be achieved with level flight stall C_L between 7–12, for practical wing loadings and installed power/weight ratios [5]. This may be a short enough runway to be competitive with vertical takeoff and landing concepts. However, there are several remaining sources of uncertainty about the viability of the SSTOL concept. These include the ability of the unblown tail to provide sufficient pitch trim and control authority, the low-speed lateral control authority of the ailerons and rudder, and the achievable three-dimensional max lift coefficient and approach angle of an aircraft with a finite wing and a realistic uneven distribution of blowing.

In order to address these uncertainties, a subscale SSTOL demonstrator aircraft was built and tested. This vehicle was designed and constructed as part of the MIT Department of Aeronautics and Astronautics senior capstone design course. This paper presents the results from initial flight tests of the aircraft, conducted during the summer of 2019.

III. Motivation

Blown wing aircraft, such as the Breuget 941 [6] or the proposed NASA X-57 [7], use wing flaps to deflect the jets of propellers arranged along the leading edge of the wing. This enhances the lift of the wing in several ways. The vertical momentum-flow change of the turned jet appears as an increased pressure load and hence an increased lift on the wing for any given angle of attack [8]. Additionally, the excess total pressure of the jet flowing through the flap slot delays the bursting of the wing main element wake, and suppresses separation over the flap [9], which increases the wing's maximum attainable lift. Depending on the vertical position of the propeller, it may also suppress separation over the main element upper surface.

Following airfoil jet-flap theory [10], the magnitude of the lift enhancement is dependent both on the momentum excess and the initial deflection angle of the jet. The excess momentum in the jet wake relative to the freestream is quantified by the airfoil jet momentum-excess coefficient,

$$\Delta c_J \;=\; \frac{2}{c}\int\left(\frac{\rho_J V_J^2}{\rho V^2}-1\right)\mathrm{d}z \;\simeq\; \frac{h_d}{c}\left(\frac{V_J^2}{V^2}-1\right)\left(\frac{V}{V_J}+1\right) \tag{1}$$

where the integral is across the jet. The approximate second expression assumes a constant density and a uniform jet, and also uses the actuator-disk result that the velocity through the disk is the average of the freestream velocity and the downstream jet velocity.

Although a large Δc_J enables large c_ℓ values, it also tends to produce high excess thrust (or negative net drag), and in fact Δc_J is nearly the same as the conventional propeller thrust coefficient for $V_J/V \gg 1$. This thrust is desirable on takeoff but not during landing, when the vehicle must be descending and thus must have positive net drag. For this reason, landing approach is an especially critical flight phase, and blown lift is only useful to reduce total field length if high lift coefficients can be generated simultaneously with positive net drag. In general, this requires large flap deflections to be used in flight. Because of the ambiguities in differentiating between thrust and drag in a blown wing system, it is convenient to examine instead the net streamwise force $X = D - T$; this is typically represented using the dimensionless coefficient C_X defined by (2). When drag is greater than thrust, C_X is positive; when thrust is greater than drag, C_X is negative.

$$C_X \;=\; \frac{X}{qS} \;=\; \frac{D-T}{qS} \tag{2}$$

The ability of the flaps to effectively deflect the flow is critical to the performance of a blown wing, since the more effective the turning the more added lift can be generated for a given amount of power, which reduces the excess thrust required to generate that lift. This effectiveness depends on the flap configuration, with more flap elements and slots being naturally more effective. Another factor is the height of the jet relative to the airfoil or flap chord, with smaller jet heights being more effectively deflected as shown by previous static testing of blown wings [11]. Distributed electric propulsion makes using many small propellers practical, and the resulting small jet heights improve flap effectiveness to the point where a simply-hinged single slotted flap may have adequate high-lift performance. Using distributed electric propulsion for blown lift naturally reduces the mechanical complexity, weight and cost of the high-lift system compared to previous blown lift aircraft. To gain an initial understanding of how well a distributed propulsion blown wing performs, a flight test vehicle was designed, built, and flown as described below.

IV. Vehicle Description

The flight test vehicle was a nominal 30% scale model of a 4-passenger SSTOL configuration described in [1]. Figure 1 gives an overview of the vehicle. To provide both high lift and cruise power, eight motors were arranged along and under the wing leading edge. The wing had three control surfaces on each side: an aileron at the tip and two single-slotted flaps inboard. The empennage consisted of conventional horizontal and vertical stabilizers.

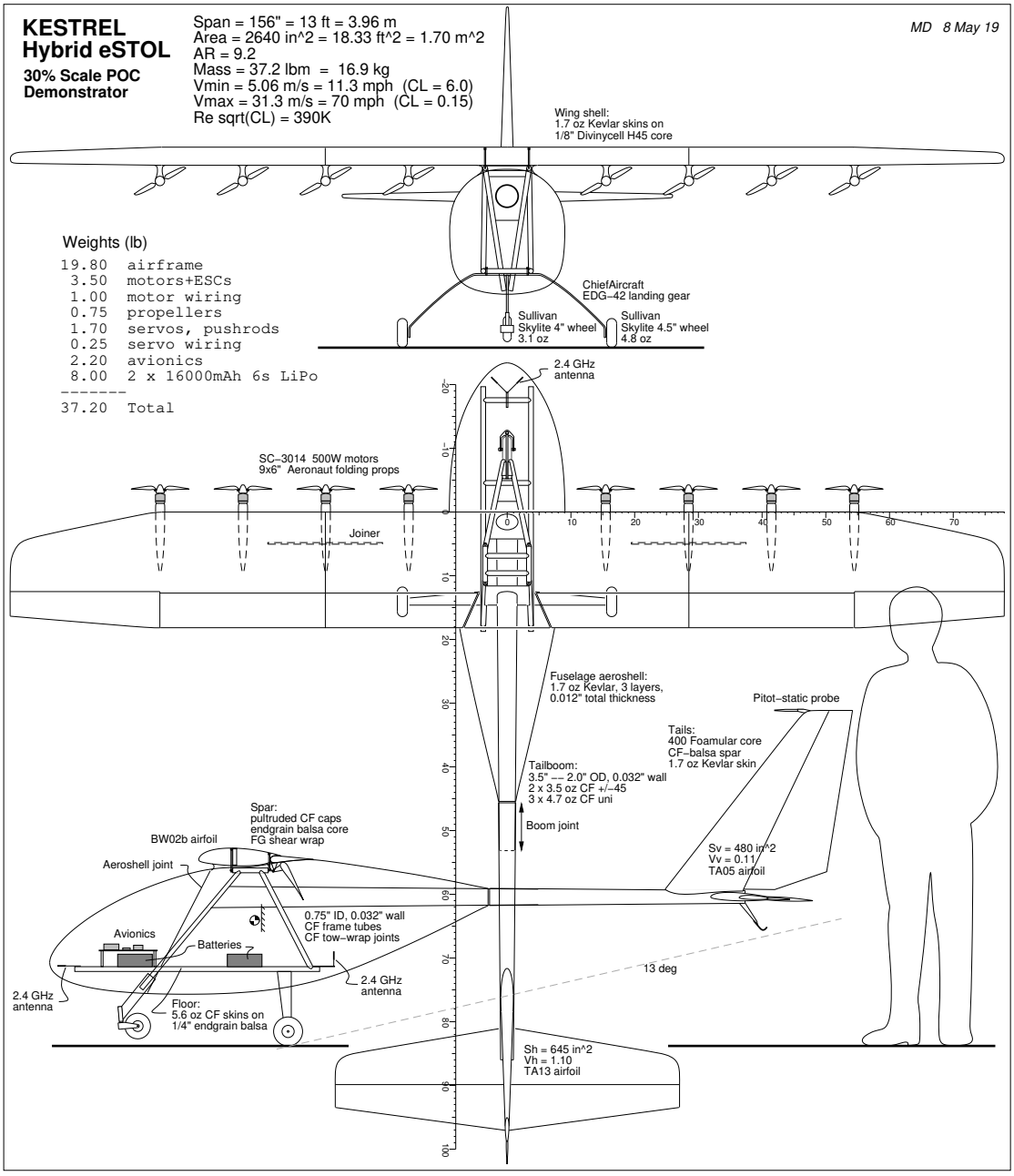

Fig. 1 Layout and internal components of the 30% STOL demonstrator aircraft, Large Propeller configuration. As-built weights and dimensions are shown.

The customized wing airfoil design was the same as tested in [4], with a 15% maximum thickness and a 38% chord flap. A cross section is shown in Figure 2. The flap hinge was well below the airfoil chord line and the main element upper surface covers the flap back to 70% chord, so that a slotted flap geometry was obtained when the flap was deflected. The wing had a 1.5 ft center chord, and a 13 ft span, with the slotted flapped airfoil extending out to 70% of the semispan. Conventional (non-slotted) ailerons extended over the outer 30% of the semispan.

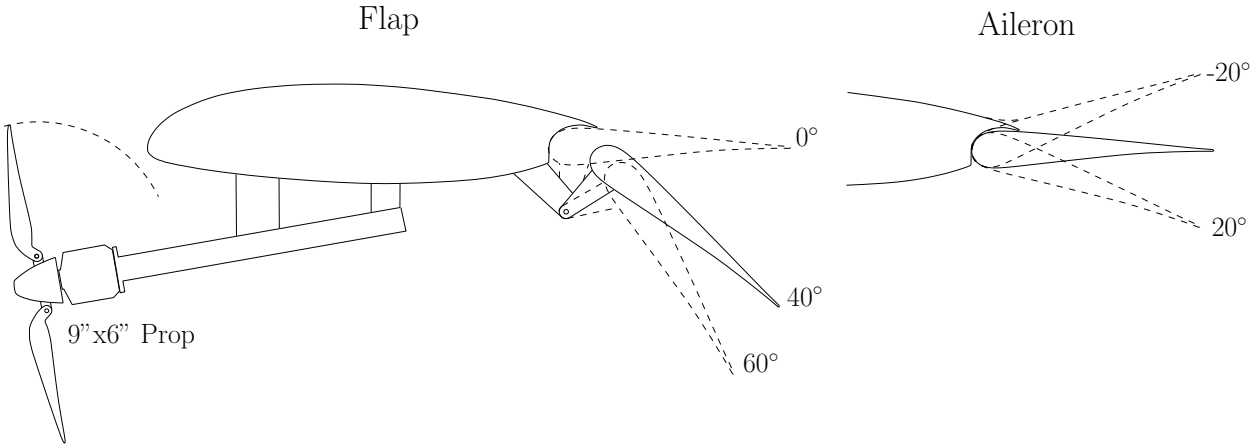

Fig. 2 A cross section of the wing showing the motor placement, as well as the different hinge locations for the inboard flap (left) and outboard aileron (right).

The all-electric powertrain consisted of mostly COTS components. Propulsive power was provided by two 6S, 16Ah LiPo battery packs supplied by MaxAmps. Each motor was a Scorpion SII-3014-830 kV, rated for 550W, powered by a YEP 40A ESC mounted just behind the motor, and directly driving a folding propeller supplied by Aeronaut.

Two different configurations of the aircraft were flown. The first used 2-blade 9" dia and 6" pitch propellers, and the second used 5-blade 7" dia and 6" pitch propellers. Foldable propellers were used in both cases. The smaller diameter props were installed for the second configuration to reduce the diameters of their jets, which could then be turned more effectively by the 35% chord flaps. The objective was to increase the maximum attainable lift, and to increase the net positive drag at large flap deflections to enable descent and landing at high blowing power.

Blade-element theory analysis of two propellers predicted that the two configurations would have similar static thrust. However, possibly due to error in the manufacturing of the custom 5-bladed hubs that reduced the effective blade pitch, the measured static thrust decreased from 0.7 to 0.45 when the smaller propellers were fitted, with the same motor/ESC/battery combinations. The maximum static thrust was measured on the ground with all 8 motors running with flaps up, although in practice the flaps were set to 25° for takeoff.

This static thrust discrepancy is still being investigated. As discussed below, the two different propellers were characterized in a wind tunnel, so this discrepancy does not affect the accuracy of the test data. The key differences between the configurations are summarized in Table 1.

Table 1 Key differences between flight test configurations

	Large Propeller	Small Propeller
GTOW (lbs)	37.2	38.9
Propeller Diameter (in)	9	7
Nominal Propeller Pitch (in)	6	6
Number of Blades	2	5
Propeller Manufacturer	Aeronaut	Aeronaut
Static T/W	0.7	0.45
Angle of Attack Sensor	No	Yes
prop diameter/flap chord	0.76	0.97

The flying weight with two battery packs was 37.2 lb in the Large Propeller configuration, and 38.9 lb in the Small Propeller configuration. The vehicle was sized to be below the 55 lb FAA limit, and was constructed primarily of composite materials. The aircraft structure was sized for a 10g (550 lb) maximum vertical load due lift or landing impact. To allow transport, the aircraft could be disassembled into the main fuselage pod, the tailboom with vertical tail, the horizontal tail, and 3 separate wing pieces. The wing-panel spars were constructed from carbon fiber and fiberglass with a balsa core, and the wing shell was a Kevlar/Divinycell sandwich. Plywood ribs close off the hollow wing panels and provide hard points for the motor mounts. The fuselage primary structure was built from carbon fiber tubes, and wass enclosed in an aeroshell made of Kevlar with balsa and carbon stiffening stringers. The tailboom wass a large-diameter carbon fiber tube. The horizontal and vertical tails had a foam core with balsa and carbon spars, with a Kevlar skin. The landing gear struts were also carbon fiber.

Flight control of the vehicle was done using a standard RC ground controller and two receivers, one located in the nose and one at the rear of the fuselage. COTS servos were used for control surface actuation. A Pixhawk 2.0 was installed to act as a data logger and telemetry system; it acted as a pass-through for the RC command signals received from the ground controller. Two additional 2S, 2.2Ah battery packs provided power for the flight control system and were independent of the main propulsion system.

The onboard instrumentation consisted of a pitot-static probe mounted at the top of the tail, a barometer and 6-DOF IMU mounted internal to the Pixhawk, and a GPS receiver. All control signals were recorded, and there was a forward-facing camera mounted at the top of the horizontal tail. Figure 3 shows the as-built vehicle in the Large Propeller configuration. In the Small Propeller configuration, a vane-type angle of attack sensor was mounted on a carbon rod cantilevered well ahead of the nose. Data logging in this configuration was switched from low-rate telemetry recorded on the ground station to onboard logging, which had substantially higher update rates. The right wing was also tufted for flow visualization.

Fig. 3 The as-built vehicle (Large Propeller) at the flight test location

Control Strategy The control strategy for this vehicle was chosen to be as conventional as possible to allow the RC pilot to safely manage the vehicle. It was designed for manual control without any stability augmentation systems apart from simple control mixing at the RC transmitter. The mixing consisted of the flap commands also driving the elevator for pitch-trim compensation, and the rudder also driven by the aileron command. This partly compensated for the extremely large adverse yaw present in high-C_L flight and thus reduced the pilot's ruddering workload. There were two motor control modes employed: Takeoff and Landing. In Takeoff mode, all 8 motors were controlled together by a single throttle lever. In Landing mode, the inner 6 motors which provide most of the blowing were controlled together via a dial knob, while the the outer two were controlled by the throttle lever. The flaps were actuated together on a single slider, and conventional Mode-2 RC transmitter stick inputs were used, with ailerons and elevator on the right stick and rudder on the left stick. In the Small Propeller configuration, the ailerons could be symmetrically drooped 10°. This was controlled via a switch and used during the takeoff roll and initial climb. Differential thrust of the outer motors was available on the ground for steering during taxiing.

V. Data Analysis Methods

The goal of the flight tests was to determine whether high-lift performance of this configuration was achievable and to assess the vehicle controllability at high-lift flight conditions. The vehicle C_L was estimated by putting the aircraft in an approximately steady flight condition;with the known weight and wing area of the vehicle the effective lift coefficient can be determined from the airspeed according to (3).

$$C_L = \frac{2W\cos\gamma}{\rho V^2 S} \tag{3}$$

Since the flight path angles were typically small it was assumed $\cos\gamma \approx 1$. This assumption was found to have little effect compared to the C_L value obtained using γ estimated from the airspeed and altitude.

The effective net streamwise force coefficient C_X is estimated from the total energy rate.

$$C_X = -\frac{\mathrm{d}E/\mathrm{d}t}{qSV} \tag{4}$$

$$E = Wh + \frac{1}{2}\frac{W}{g}V^2 \tag{5}$$

The altitude h was obtained from the onboard barometer, and indicated airspeed was measured from the pitot-static system. Since the pitot-static probe was mounted far from the body, the indicated and calibrated airspeeds were considered to be equivalent. Using (4) and (5) to compute C_X conserves energy exactly, since the beginning and end E values are unaffected regardless of how $E(t)$ is filtered before differentiation. This makes it preferable than if $h(t)$ and $V(t)$ were filtered and differentiated separately.

The altitude and airspeed data were smoothed with a 2-second moving average to compensate for sensor noise. This reduced the ability to capture fast dynamics of the vehicle but since the primary data of interest was the steady-state performance of the system this was not a significant limitation. The density was corrected for the ambient pressure and temperature recorded at nearby Lawrence airport.

The elevator deflection required to trim the vehicle, the flap deflection settings, and the aileron inputs were determined by recording the RC command signals sent to the vehicle, and correlating these with measurements taken on the ground of the various control surface deflections. Handling qualities were assessed qualitatively based on input from the flight test pilot.

For a blown wing, the lift coefficient C_L varies strongly with angle of attack α, flap deflection δ_F, and the jet momentum-excess coefficient ΔC_J. The latter represents the overall blowing intensity of all the propulsors, and can be defined by integrating the sectional Δc_J across the span [4].

$$\Delta C_J = \int_{-b/2}^{b/2} \Delta c_J \, c \, \mathrm{d}y \tag{6}$$

For this aircraft it was assumed that there was uniform blowing across the inner six motors at one throttle level, and across the outer two motors at a different throttle level. The effective ΔC_J for the total vehicle is therefore

$$\Delta C_{J_{\text{eff}}} = \frac{S_{\text{inner}}}{S}\Delta c_{J_{\text{inner}}} + \frac{S_{\text{outer}}}{S}\Delta c_{J_{\text{outer}}} \tag{7}$$

where S_{inner} is the projected wing area from the edge of the fuselage to midway between the furthest and second-furthest motors, and S_{outer} is the projected wing area in the slipstream of the outermost motor.

As can be seen from its definition (1), the local Δc_J at each spanwise station is a function of the local jet velocity, which is determined by the throttle setting of the motor (PWM command signal) and the freestream velocity. To estimate this relationship, each propeller was characterized in isolation in a 1 ft x 1 ft open jet wind tunnel with the flight motor and ESC. Thrust was measured as a function of throttle setting, across the speed range encountered in the flight tests. Jet velocity was calculated using the actuator disk relationship (8).

$$\left(\frac{V_J}{V}\right)^2 = \frac{T}{(\pi R^2)V^2\frac{\rho}{2}} + 1 \tag{8}$$

This estimation of ΔC_J via measured thrust is justified by the fact that Δc_J and the 2D propeller thrust coefficient definitions are exactly equivalent at the static condition where $V_J/V \to \infty$ and are always correlated at any other condition with finite V_J/V.

VI. Results and Discussion

The results presented here are from four separate flight tests conducted over two days at the Plum Island Airport (2B2)in Newburyport, MA. For the first two flights, on June 9, 2019, the vehicle was in Large Propeller with the larger 9" propellers. In the second two flights, on Sept 15, 2019, the vehicle was in the Small Propeller configuration with 7" propellers. All flights took place between 8 am and 11 am, with winds below 10 mph. Each flight started with fully charged batteries, and lasted 10–15 minutes. In the following sections these flights are labeled LP1–SP2 as shown in Table 2.

Table 2 Flight tests described in the following sections

Flight Number	Date	Temp (C)	Pressure (mbar)	Configuration
LP1 LP2	9-Jun	16.1	1028.4	Large Propeller
SP1 SP2	15-Sep	20	1019.3	Small Propeller

In order to keep the vehicle within visual range and under the FAA Part 107 altitude limit, the pilot kept the vehicle in close-to-level flight for most of the test. In practice, this limited the amount of power usable at low speeds to throttle settings that would not cause the vehicle to climb or accelerate. The usable throttle was observed to depended strongly on flap deflection as well the propeller size. In the LP1 and LP2 flights, full power could only be used with maximum flap deflection(60°); at the $30° - 40°$ flap settings which wind tunnel testing predicted would give the best lift enhancement [4], usable power was about 50%. This limited the amount of lift enhancement, and hence the minimum flight speed, of the vehicle.

In the SP1 and SP2 flights with the 7" propeller, the usable throttle was observed to be much higher and consequently significantly slower flight speeds were reached. This was likely because the flaps are more effective at deflecting the smaller jet, which causes an increase in the amount of lift augmentation per power. The throttle settings are not directly comparable between flights, as the Large Propeller configuration had more thrust than the Small Propeller. However, the ΔC_J coefficients can be compared directly as they account for differences in thrust and propeller size.

To limit the excess thrust and allow higher blowing power over the flaps, most of the flights took place in Landing mode, with the inner six motors controlled together and the outer two off or at low power settings. In Takeoff mode where all eight motors were controlled together, high power settings would cause the vehicle to quickly accelerate or climb.

At low flight speeds the lateral handling qualities degraded, making the vehicle difficult to control. This made it difficult to fly steady high-lift test points and take precise measurements. The results which follow illustrate the major trends observed and key findings of the tests.

A. Maximum Lift Coefficient

Figure 4 shows representative results from a high lift test point, with 44° flaps, the outer motors off, and the inner motors set to 85% throttle. The traces of measured airspeed, altitude, and angle of attack are shown, along with calculated C_L and ΔC_J. The dashed lines on the airspeed, altitude, and angle of attack plots represent the measured data from onboard the aircraft, while the solid lines show the smoother two second moving average. The smoothed value of airspeed was used for computing the C_L and ΔC_J coefficients shown. Angle of attack measurements were not corrected for the upwash induced by the wing. The typical procedure for flying a test point was to maintain a fixed flap and throttle setting and control the vehicle speed using the elevator. The pilot attempted to keep the vehicle in steady low-speed flight, as well as performing several power-on stalls. This is reflected in Figure 4. From 427 to 437 seconds in the flight (between the dashed lines) there was a period of sustained high-lift flight at an average C_L of 7.5. Higher stall C_L values, of 15.5, 12.4, and 13.3, were observed around 453, 460 and 480 seconds respectively. Due to the poor low-speed handling qualities of the vehicle it was difficult to fly steady high C_L test points. At the slowest flight speeds, it was observed by the pilot that most of the available elevator input was required to trim the vehicle. This, combined with the poor lateral control, meant that the vehicle could not be held near the stall point for a significant period of time.

The uncertainty in the data collection also becomes significant at low airspeeds. As mentioned, the lift coefficient was estimated based on the current indicated airspeed and the assumption of steady flight. At very low airspeed, the

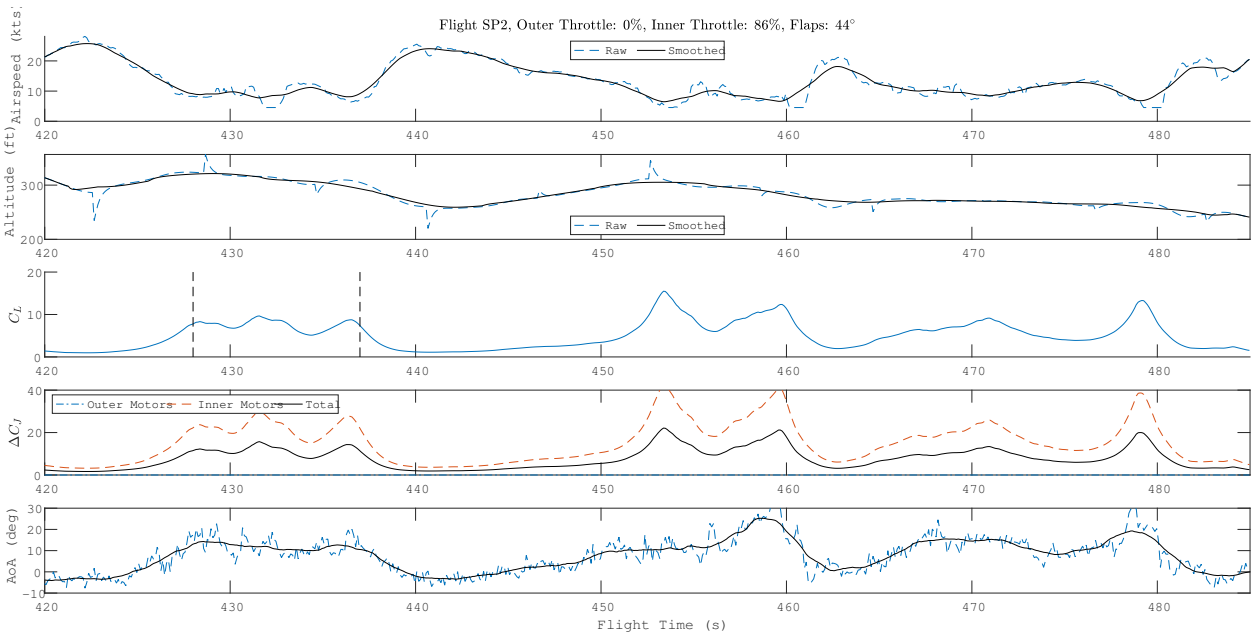

Fig. 4 Flight test data for the SP2 configuration with 44° flap deflection and the inner throttle set to 86%.

pitot tube being used gave unreliable readings, at times reading zero or close to it. In order to prevent these readings from unduly distorting the moving average, a minimum airspeed of approximately 5 kts was assumed. This corresponds to twice the resolution of the pressure transducer used in the pitot tube, which was 0.84 Pa. Any uncertainty in the probe is magnified at very low speed, so there is more uncertainty in the largest estimated flight C_L values. Additional sources of error also increase in significance at low airspeeds. For example, the maximum C_L at 453 seconds was not associated with an increase in the vehicle angle of attack, but the airspeed at that point dropped to the minimum value. This may indicate a tailwind gust momentarily reduced the indicated airspeed measurement. Uncertainty also arises from installation effects on the pitot probe, and the unknown load factor or bank angle of the aircraft. Additional work and improved instrumentation is required to quantify and reduce these error sources.

Another way to examine the available data is as a plot of C_L versus angle of attack measured in flight, shown in Figure 5 for the second set of flight tests (Flights SP1 and SP2); these had the best high-lift performance. Each plot encompasses the entire range of flap deflections and throttle settings used in the flight, which accounts for the spread in the data-point traces. The color of each dot represents the effective ΔC_J of the inner motors, as this is expected to be

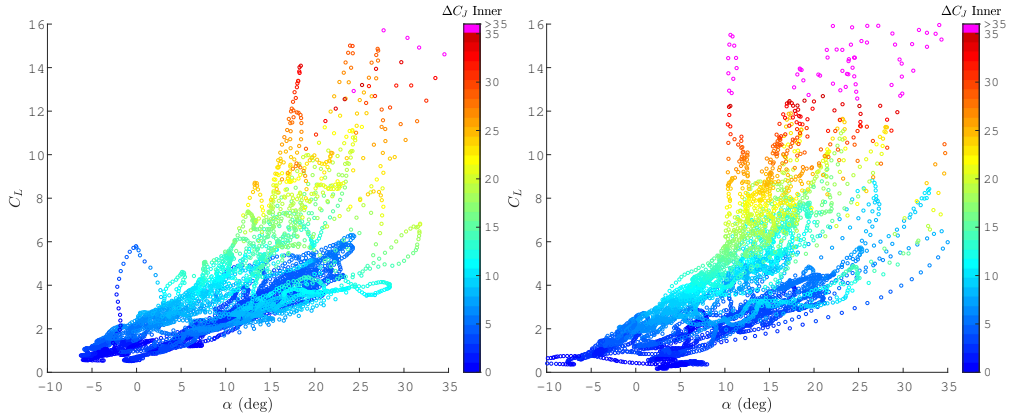

(a) Flight SP1 **(b) Flight SP2**

Fig. 5 Flights SP1 and SP2, with the smaller 7" propellers, demonstrated the best high-lift performance, with maximum lift coefficients above 10 repeatedly observed.

most strongly correlated with the lift augmentation. Because of the very large ΔC_J values obtainable at low airspeed, any ΔC_J over 35 is shown in magenta to prevent outliers from distorting the color scale. This is done on all subsequent plots which use color to represent ΔC_J.

While there are some outliers that may be the result of measurement error or may not be trimmable for steady flight, $C_{L_{\max}}$ values in excess of 10 are repeatably observed. This is within the range of stall lift coefficients required to achieve the desired short-field performance [5] [1]. It is not clear what the maximum lift coefficient is because of the high uncertainty in the slow-speed measurement and the difficulty of low-speed flight control. However, these results suggest that acceptable controllability, and not aerodynamic stall of the wing, is the factor which determines the lowest flight speed of the vehicle. Where this limit lies precisely is dependent on the details of the aircraft and control system design.

B. Effects of Flap Deflection

The data shown in Figure 5 can be refined by only showing points corresponding to specific flap deflections. Figure 6 shows the $C_L - \alpha$ curves for selected flap deflections in Flights SP1 and SP2. The best lift augmentation is observed at 34°; this is in agreement with the results of the wind tunnel testing which showed 40° flaps having the best high lift performance [4]. It can also be seen that, as expected, increasing ΔC_J or α increases the lift of the wing. Figure 6(a) shows the largest flap deflections are not effective at generating high lift coefficients due to separation of the flow from the flap. An image of this separation is shown in Figure 7. High flap settings are also desirable on approach because they allow high lift, high drag flight conditions. This can be seen from Figure 12 in the Appendix, where the additional drag from larger flap deflections allows more usable throttle and hence higher lift coefficients with positive C_X (net drag). This is true for both the Large Propeller and Small Propeller configurations.

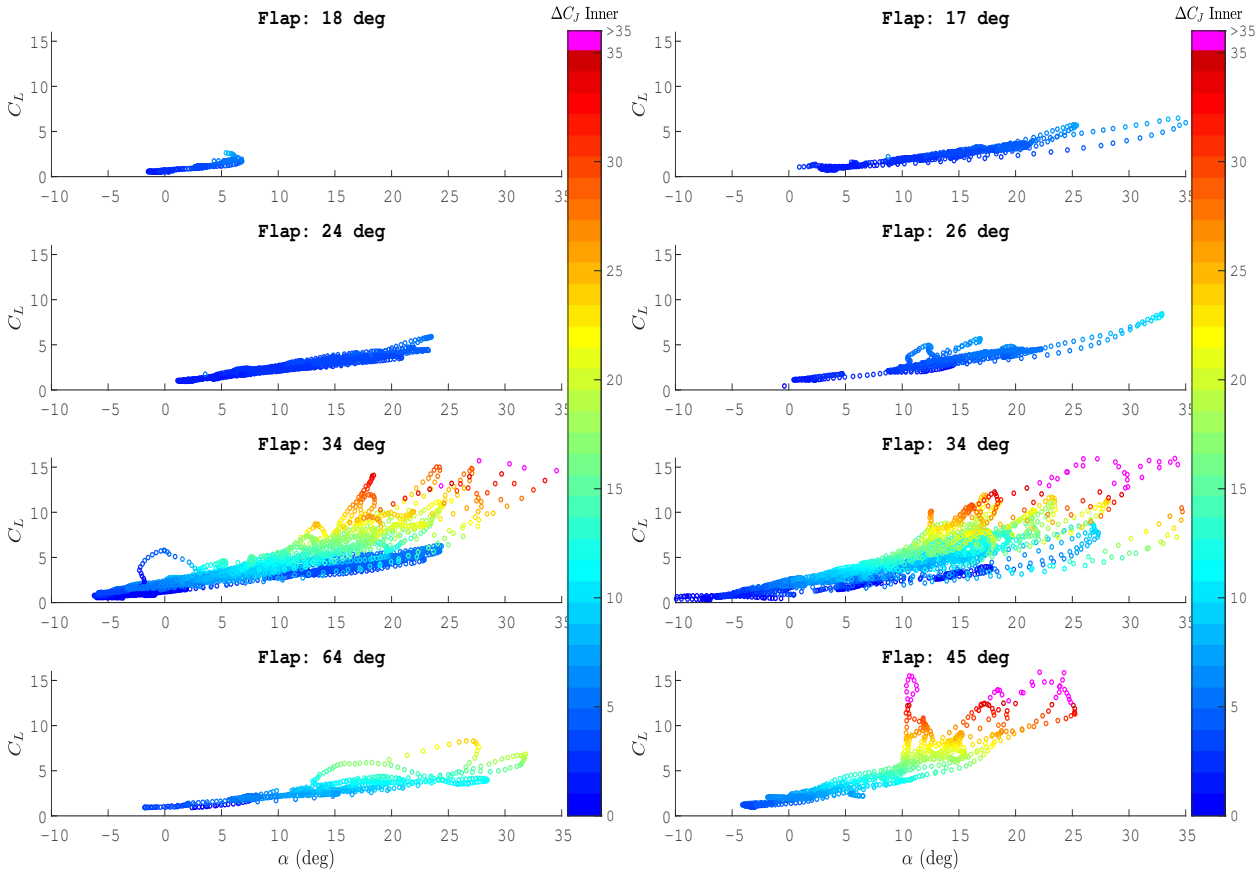

(a) Flight SP1 **(b) Flight SP2**

Fig. 6 Examining specific flap deflections illustrates how higher flap deflections enable higher lift coefficients to be achieved in level flight, up to the point where the flow separates from the flap.

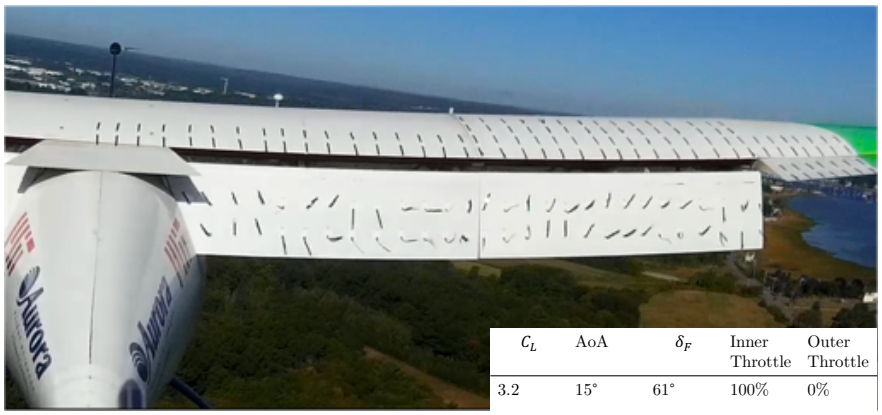

Fig. 7 Separation of the flow over the flaps was observed at high flap deflections (61°), even with high blowing.

C. Effect of Changing Propeller Diameter

It was observed that the Small Propeller configuration was able to achieve substantially higher lift coefficients in level flight than the Large Propeller configuration. This is shown best in Figure 12, which shows the C_L–C_X polar from the LP2 (left) and SP2 (right) flight tests for the 36° and 34° flap deflections, respectively. These plots show the C_L at every point plotted against the C_X at the same point estimated from the energy state. Color represents ΔC_J as in the previous plots. Since the Large Propeller test flights did not have an angle of attack probe equipped, the C_L-α curves cannot be compared directly. The increased point density in Figure 8 (b) is due partially to the high logging rate with the onboard data relative to the telemetry.

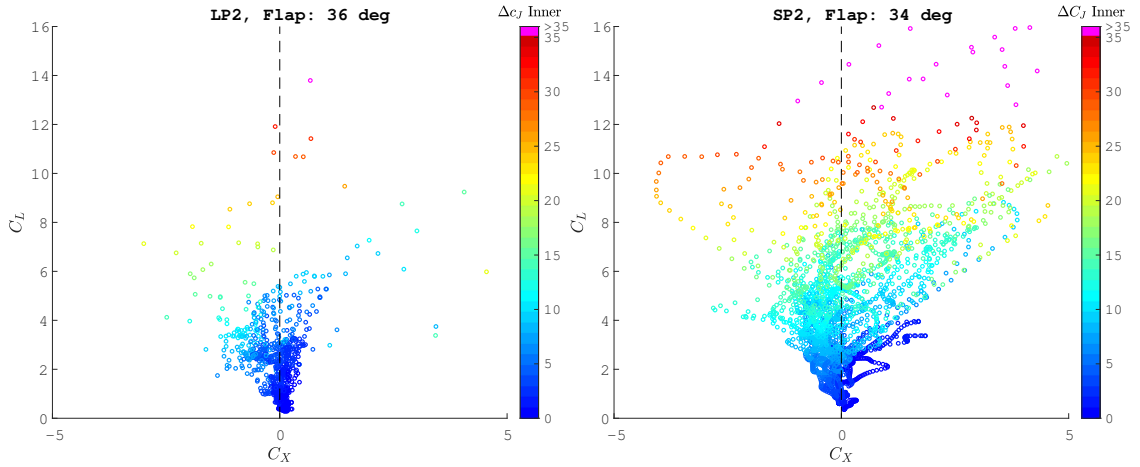

(a) Flight LP2 **(b) Flight SP2**

Fig. 8 Flight SP2 (right) demonstrates improved high-lift performance relative to the Flight LP2 (left) because the smaller propeller jet is more effectively turned by the flaps, enabling more lift to be generated with less excess thrust

Comparing Figure 8(a) with Figure 8(b) it can be seen that higher lift coefficients with positive C_X (net drag) are repeatably achievable in Figure 8(b), with the 7" propeller. In Figure 8(a), higher ΔC_J is associated with negative C_X (positive thrust) at most C_L. As mentioned, this is likely due to the fact that the flaps are more effective at deflecting the smaller jet wake. The improved turning of the jet increases the lift augmentation for a given angle of attack and ΔC_J. This means that lower ΔC_J is required for a given C_L, which also implies a lower excess thrust (or higher C_X). This allows the pilot to use higher power settings while maintaining level flight, which increases the C_L that is achievable in flight. This agrees with pilot observations that much more throttle could be used, and lower flight steady flight speeds therefore achieved, without the airplane climbing in the Small Propeller configuration. It should be noted that ΔC_J and

C_X, for a fixed power and flap setting, will vary significantly with changing angle of attack and airspeed; this accounts for the spread in C_X values around 0; higher C_X for a given C_L corresponds to higher angle of attack and lower power setting. For most of the test points the outer motors were off, but in some cases low power was used to improve lateral control, which also impacts C_X. This results shows the relative size of the wing, flaps and the propeller is significant to the performance of a blown lift aircraft. Continued research into this design space is important for improving the performance of blown wing aircraft.

D. Takeoff Performance

The takeoff procedure was for the pilot to hold full back elevator and apply full throttle, while a second person held the tail of the aircraft. After the aircraft reached full power the pilot signaled for the tail to be released. Takeoff flaps were varied between 20 and 25 degrees. A composite photo of the takeoff from Flight LP2 is shown in Figure 9.

Fig. 9 In the Large Propeller configuration with 25° flaps, the vehicle demonstrates a takeoff roll of 2.0–2.5 vehicle lengths, and a maximum climb-out angle of 21 deg.

The aircraft had a slightly nose-down ground roll attitude, and the nearly level liftoff attitude. This indicates that the takeoff distance of the aircraft was limited by the rotation rate that the unblown tail is able to generate at low airspeed. Table 3 shows the takeoff lift coefficients were relatively low relative to what the vehicle was able to generate in other phases of flight. In flights SP1 and SP2, the takeoff angle of attack was close to zero. Ideally, takeoff would occur at higher angle of attack and lower speeds, but the aircraft could not rotate quickly enough to get to a high angle of attack before accelerating to a higher speed, enabling takeoff at a lower lift coefficient.

Flight	$C_{L_{\mathrm{TO}}}$	α_{TO}	$\delta_{F_{\mathrm{TO}}}$
LP1	1.9	-	20.3°
LP2	2.1	-	24.8°
SP1	3.4	0.54°	24.3°
SP2	2.6	-1°	25.7°

Table 3 Takeoff parameters for each flight

This suggests that the ground roll of this aircraft is limited by the control power of the horizontal tail. There is an opportunity to shorten the takeoff distance by changing the ground roll attitude of the aircraft, increasing the tail volume, increasing the incidence angle of the wing, or increasing the takeoff flap deflection. However, the resulting increase in achievable C_L or decrease in takeoff α must be balanced with the increase in drag during the ground roll segment. While the takeoff ground roll was not measured precisely, there was little apparent change in performance between the Large and Small Propeller configurations; the reduction in excess thrust was partially compensated for by the reduced takeoff speed but the horizontal tail authority was unchanged. Because of the difficulties in controlling the aircraft, tests of high-lift approach and landing were not undertaken.

E. Handling Qualities

As mentioned, at low airspeed the vehicle was difficult to control due to low dynamic pressure over the control surfaces. At the high flap deflections and high C_L, the flaps induce an upwash on the wing immediately ouboard of the flap ends, which would tend to induce a stall at that location. As a result a significant portion of each aileron was in separated flow, reducing the roll control authority. When the outboard two motors were running, the separation over the inboard portion of the aileron was suppressed, improving handling somewhat. This is shown in Figure 10. In the top image, with the outer motors off, separation of the flow over the main element can be seen across the whole span of the aileron. With the motors running, shown on the bottom, only the outer half of the aileron has separated flow.

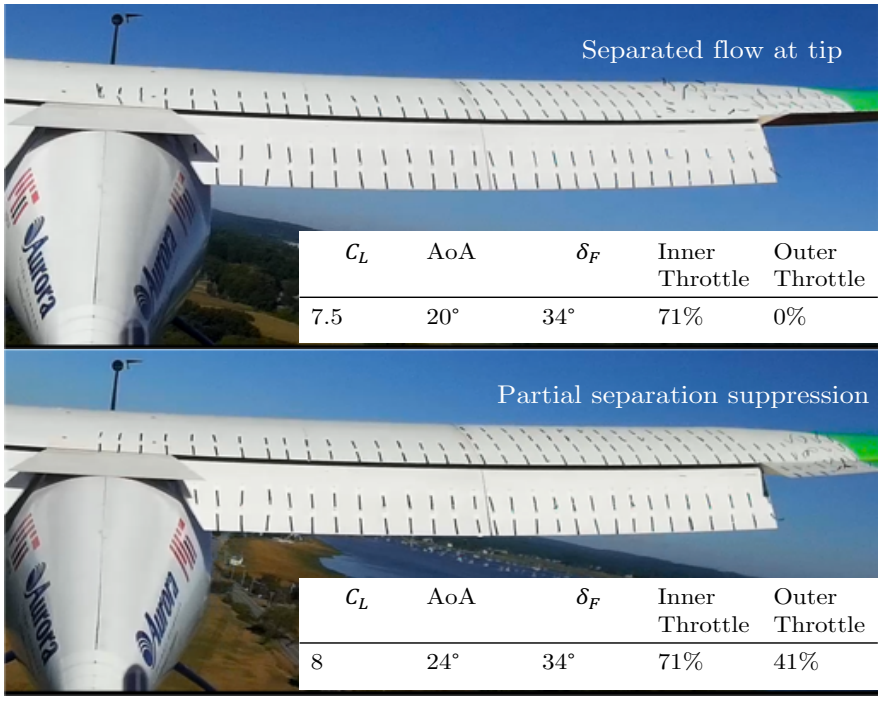

C_L	AoA	δ_F	Inner Throttle	Outer Throttle
7.5	20°	34°	71%	0%

C_L	AoA	δ_F	Inner Throttle	Outer Throttle
8	24°	34°	71%	41%

Fig. 10 When the outer motor is off, separation appears near the flap/aileron break and over the tip (top). When the outer motors at the break are blowing, this separation is partly suppressed(bottom).

During low-speed flight large elevator inputs were required to trim the vehicle, approaching the maximum travel of the elevator. The ability to trim the aircraft may limit the achievable high lift coefficients. Redesigning the tail, either by increasing the tail volume, elevator area, or an all-flying tail, may reduce the speed further. The effect of blowing on the flow at the tail, both the effective dynamic pressure and downwash angle, also requires further study.

Additionally, the more complex control setup of two throttle controls as well as flaps made managing the vehicle flight path on descent challenging, which compounded the lateral control difficulties. Control strategies for this aircraft, both in how to generate sufficient control authority and how to translate pilot inputs into actuator movements, are an important area of research going forward. It should be emphasized that there are various techniques that have been shown to enhance the lateral control of blown lift aircraft, including fully outboard flaperons, spoilers, and differential thrust [6]. None were implemented on this vehicle, but they offer several paths towards improving lateral handling qualities in subsequent aircraft.

F. Partial Flap Separation

An interesting phenomena observed during SP2 was lateral variation in the flow separation over the flap at a large flap deflection, shown in Figure 11. In this condition, the outer motors are shut off, while the inner six are operating at 80% throttle, which corresponds to a $\Delta c_{J_{\text{inner}}} = 9.1$ at a flight speed of 12 kts. The exact reasons for this partial separation are not known, although it may be related to spanwise variation in jet velocity. Further investigation here is needed, but this does suggest that the assumption that the propeller wake spreads out evenly into a uniform jet may not be valid. In the Small Propeller configuration the spacing between the motors was larger than originally designed due to

the reduction in motor diameter. It is unknown whether this partial separation also occurred during the Large Propeller configuration flight tests, as the wing was not tufted for those tests.

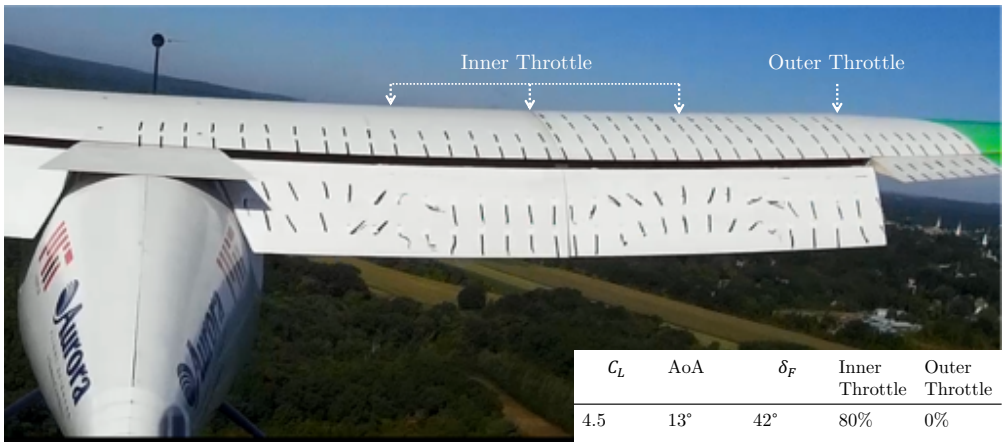

Fig. 11 Lateral variations in flow separation over the flap. Arrows indicate the location of the motor centerlines.

VII. Conclusion

The initial conclusion from the flight tests is that the vehicle can achieve flight $C_{L_{\max}}$ values in excess of 10, but that vehicle control at the low airspeeds reached was marginal with the mostly conventional control arrangement used. Partial blowing of the ailerons was observed to improve lateral handling qualities, but even with partial blowing control of the vehicle was still difficult. Large elevator inputs were also required to trim the vehicle in pitch. The minimum flight speed of this aircraft is likely not limited by aerodynamic stall of the wing, but by the ability of the pilot to trim and control the vehicle at low speeds. Several approaches, which are not implemented on the current aircraft, exist which have been shown to improve the lateral and longitudinal control authority.

The size of the propeller diameter was shown to be important to achieving high lift with low excess thrust. Specifically, the smaller jet of a smaller propeller is turned more effectively by the flap, resulting in an increase in lift for a given power. Further research into the relationship between propeller size, wing and flap size, and achievable C_L and C_X is needed. Achievable rotation rate during the ground roll was found to play a significant factor in determining the takeoff distance of the vehicle. These results show there is promise to the distributed electric propulsion blown lift concept but that there is a need for further work on vehicle control strategies.

Acknowledgments

This work was supported by Aurora Flight Sciences: A Boeing Company. The authors would like would acknowledge the assistance of Tony Tao, as well as Trevor Long and Annick Dewald for their work characterizing the motors and propellers used in the flight test. Finally, this project would not have been possible without the hard work of the members of the MIT Aeronautics and Astronautics senior design class who designed and and built the vehicle; we are grateful for all their effort.

A. Additional Polars

Figure 12 below shows the C_L-C_X polars for all four flight tests, for four representative flap deflections. The exact same flap deflections were not used during each flight, as there were no detents on the slider used to control flap position.

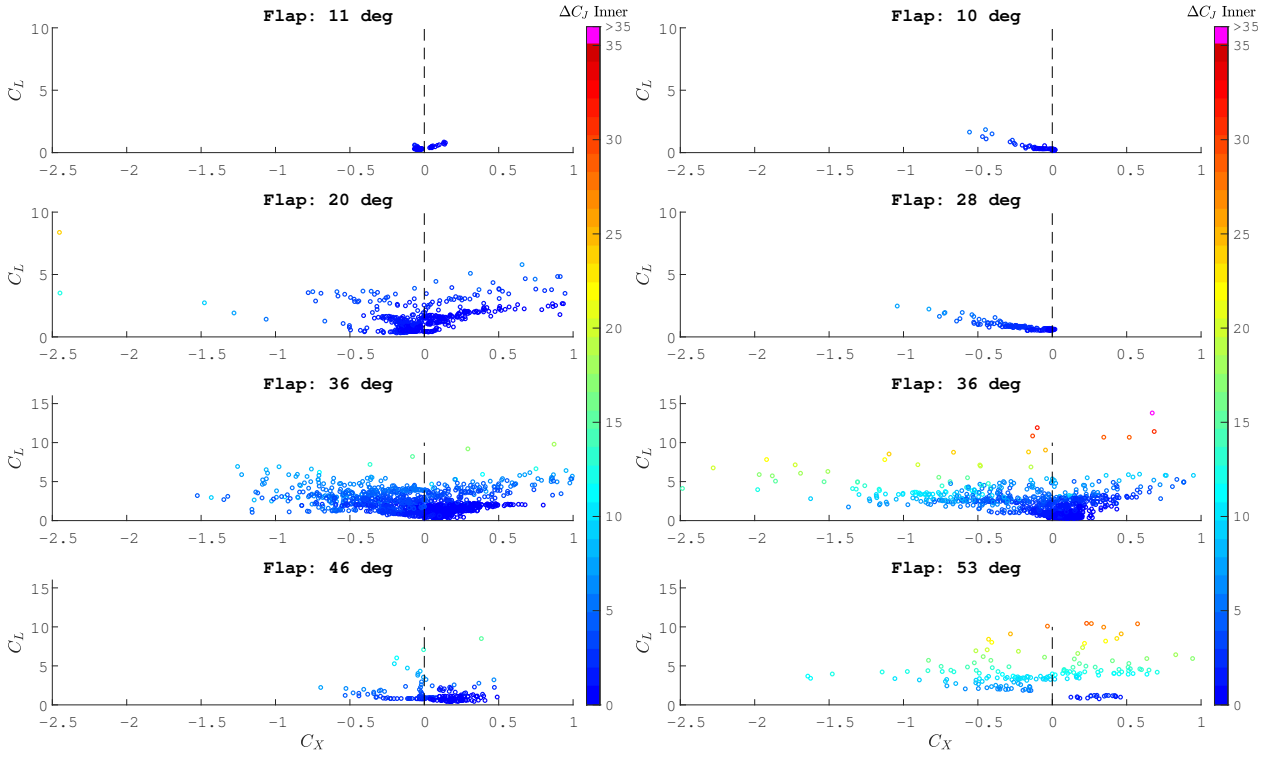

(a) Flight LP1, 9" Propeller

(b) Flight LP2, 9" Propeller

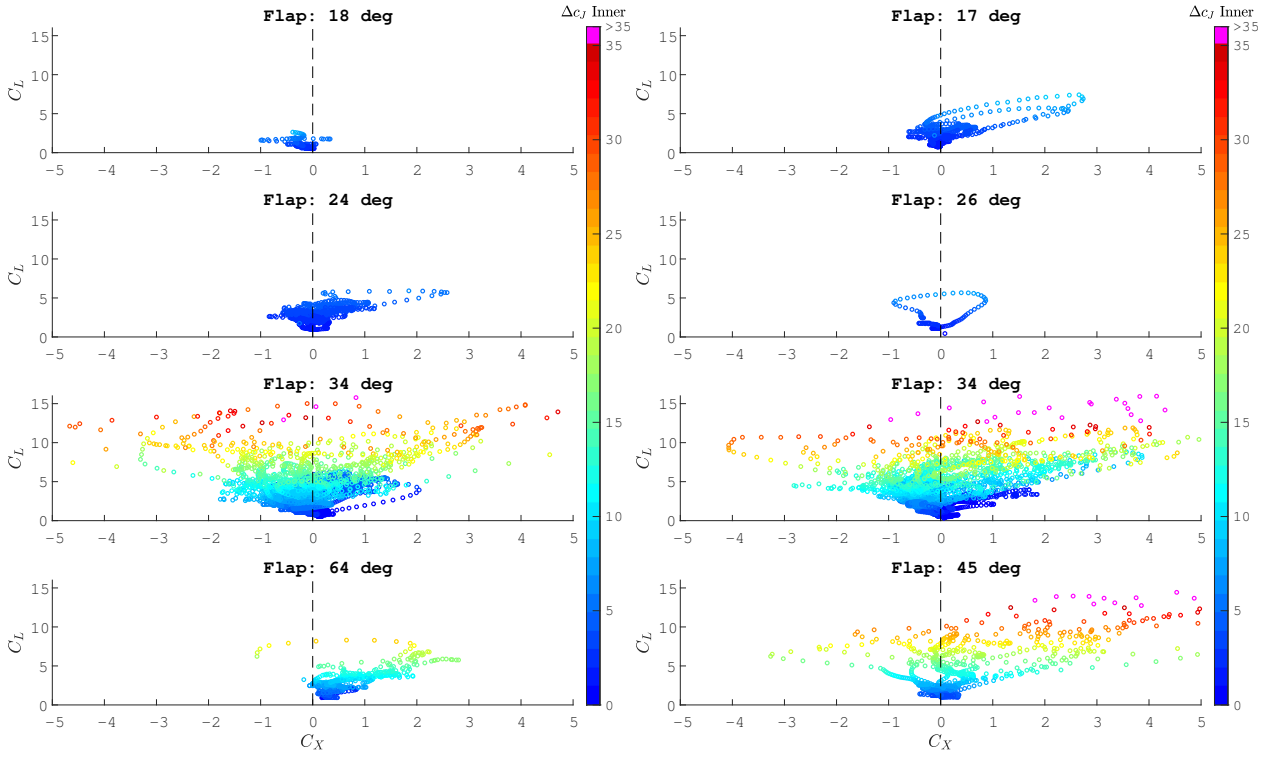

(c) Flight SP1, 7" Propeller

(d) Flight SP2, 7" Propeller

Fig. 12 Switching to smaller 7" propellers enables higher lift coefficients and higher jet momentum-excess coefficients to be reached in steady flight

References

[1] Gnadt, A., Isaacs, S., Price, R., Dethy, M., and Chappelle, C., "Hybrid Turbo-Electric STOL Aircraft for Urban Air Mobility," *AIAA Scitech 2019 Forum*, American Institute of Aeronautics and Astronautics, Reston, Virginia, 2019. doi:10.2514/6.2019-0531, URL https://arc.aiaa.org/doi/10.2514/6.2019-0531.

[2] Courtin, C., Burton, M. J., Yu, A., Butler, P., Vascik, P. D., and Hansman, R. J., "Feasibility Study of Short Takeoff and Landing Urban Air Mobility Vehicles using Geometric Programming," *2018 Aviation Technology, Integration, and Operations Conference*, 2018, p. 4151.

[3] Courtin, C., and Hansman, R. J., "Safety Considerations in Emerging Electric Aircraft Architectures," *2018 Aviation Technology, Integration, and Operations Conference*, 2018, p. 4149.

[4] Agrawal, D., As'ad, F., Berk, B., Long, T., Lubin, J., Courtin, C., Thomas, J., Drela, M., and Hansman, R. J., "Wind Tunnel Testing of a Blown Flap Wing," *2019 Aviation Technology, Integration, and Operations Conference*, 2019.

[5] Courtin, C., "An Assessment of Electric STOL Aircraft," Master's thesis, Massachusetts Institute of Technology, 2019.

[6] Quigley, H., Innis, R., and Holzhauzer, C., "A Flight Investigation of the Performance, Handling Qualities, and Operational Characteristics of a Deflected Slipstream STOL Transport Airplane Having Four Interconnected Propellers," Technical Note NASA TN D-2231, NASA, Mar 1964.

[7] Viken, J.K. et al., "Design of the Cruise and Flap Airfoil for the X-57 Maxwell Distributed Electric Propulsion Aircraft," AIAA-2017-3922, Jun 2017.

[8] McCormick, B. W., *Aerodynamics of V/STOL Flight*, Academic Press, 1967.

[9] Roe, M. H., and Renselaer, D. J., "STOL Tactical Aircraft Investigation, Externally Blown Flap. Volume II. Design Compendium," Tech. rep., Rockwell International Corporation, 1973.

[10] Spence, D., "The lift coefficient of a thin, jet-flapped wing," Tech. rep., 1956. URL https://royalsocietypublishing.org/doi/pdf/10.1098/rspa.1956.0203.

[11] Kuhn, R. E., "Semiempirical Procedure for Estimating Lift and Drag Characteristics of Propeller-Wing-Flap Configurations for Vertical-and Short-Take-Off-and-Landing Airplanes," 1959. URL https://ntrs.nasa.gov/search.jsp?R=19980232082, nASA MEMO 1-16-59L.